DOI 10.1007/s11182-018-1307-8

Russian Physics Journal, Vol. 60, No. 11, March, 2018 (Russian Original No. 11, November, 2017)

MAGNETIC PROPERTIES AND STRUCTURAL CHARACTERISTICS OF $BaFe_{12}O_{19}$ HEXAFERRITES SYNTHESIZED BY THE ZOL-GEL COMBUSTION

V. A. Zhuravlev,[1] V. I. Itin,[2] R. V. Minin,[2] Yu. M. Lopushnyak,[1] and D. A. Velikanov[3]

UDC 538.62, 548:537.611.46

The phase structure, structural parameters, and basic magnetic characteristics of $BaFe_{12}O_{19}$ *hexaferrites prepared by the zol-gel combustion method with subsequent annealing at a temperature of 850°C for 6 h are investigated. The influence of the organic fuel type on the properties of synthesized materials is analyzed. Values of the saturation magnetization and the anisotropy field are determined. It is established that they depend on the organic fuel type. It is shown that powders synthesized with citric acid used as a fuel have the largest particle sizes and the highest saturation magnetization.*

Keywords: zol-gel combustion method, nanostructured hexaferrites, magnetization curve, saturation magnetization, ferromagnetic resonance, magnetocrystalline anisotropy.

Oxide ferrimagnets with hexagonal crystal structure (hexaferrites) are widely used in different fields of modern technology. According to [1], nowadays the number of publications devoted to investigation of physical properties and various aspects of hexaferrite applications grows exponentially. The unique hexaferrite properties are caused by large values of magnetocrystalline anisotropy (MCA) and high magnitudes of saturation magnetization fields [2]. Recently new energy-saving methods of synthesizing nanostructured hexagonal oxide ferrimagnets have been suggested, including self-propagating high-temperature synthesis (SHS), mechanochemical method of synthesis from salt systems, zol-gel method, and some others [1].

In the present work, the zol-gel combustion is used to produce $BaFe_{12}O_{19}$ nanostructured barium hexaferrite powders of M-type (Ba-M). The influence of the organic fuel type on the structural and morphological characteristics of powders and their magnetic properties is investigated. Aqueous solutions of barium nitrate $Ba(NO_3)_2$ and iron nitrate 9-water $Fe(NO_3)_3 \cdot 9H_2O$ with concentration of 1 M were used as reagents, and aqueous solutions of carbamide $CO(NH_2)_2$ (sample No. 1), sucrose $C_{12}H_{22}O_{11}$ (sample No. 2), glycine $C_2H_5NO_2$ (sample No. 3) and citric acid $C_6H_8O_7$ (sample No. 4) also with concentration of 1 M were used as organic fuels. The formation of Ba-M hexaferrite nanoparticles after zol-gel combustion process was completed by annealing of the powders at 850°C for 6 h. The procedure of synthesizing Ba-M nanostructured powders by this method was described in [3].

A polyctystalline RIGAKU ULTIMA 4 diffractometer was used for x-ray phase analysis and x-ray structural analysis (XRPA and XRSA) of samples under programs of full-profile analysis (Rigaku Corp.) and *Powder Cell 2.4*. Sizes of coherent scattering regions (CSR) were calculated based on an analysis of physical diffraction line broadening

[1]National Research Tomsk State University, Tomsk, Russia, e-mail: ptica@mail.tsu.ru; lum83@mail.ru; [2]Department of Structural Macrokinetics of the Tomsk Scientific Center of the Siberian Branch of the Russian Academy of Sciences, Tomsk, Russia, e-mail: waserman@yandex.ru; [3]L. V. Kirensky Institute of Physics of the Siberian Branch of the Russian Academy of Sciences, Krasnoyarsk, Russia, e-mail: dpona1@gmail.com. Translated from Izvestiya Vysshikh Uchebnykh Zavedenii, Fizika, No. 11, pp. 87–94, November, 2017. Original article submitted July 14, 2017.

TABLE 1. Results of XRPA and XRSA of Samples after Zol-Gel Combustion and Thermal Treatment at 850°C for 6 h

Phase	Phase content, mass%	Lattice constant, Å		CSR, nm
		a	*c*	
Sample No. 1				
$BaFe_{12}O_{19}$	76.8	5.9035	23.3130	60
α-Fe_2O_3	23.2	5.0508	13.7837	69
Sample No. 2				
$BaFe_{12}O_{19}$	94.0	5.9157	23.3269	45
α-Fe_2O_3	5	5.0563	13.8061	62
Fe_3O_4	1.0	8.4667	–	30
Sample No. 3				
$BaFe_{12}O_{19}$	94.1	5.9050	23.3130	61
α-Fe_2O_3	4.0	5.0478	13.7865	56
Fe_3O_4	1.9	8.3818	–	24
Sample No. 4				
$BaFe_{12}O_{19}$	92.2	5.9170	23.3302	83
α-Fe_2O_3	7.8	5.1216	13.7035	24

using Scherrer's formula commonly used to estimate the nanoparticle sizes. According to Table 1 in which the XRPA and XRSA results are presented, along with the $BaFe_{12}O_{19}$ target phase, the samples contain α-Fe_2O_3 impurity hematite phase and traces of magnetite Fe_3O_4 phase.

Sample No. 1, prepared using carbamide $CO(NH_2)_2$, contained the least amount of the target phase (≈77%). The content of the Ba-M phase for the remaining samples exceeded 92%. The synthesized materials had close values of the lattice constants *a* and *c* of the target and impurity phases, respectively. The values of the lattice constants were close to those presented in [2].

From the last column of Table 1 it can be seen that sizes of nanoparticles synthesized with the use of citric acid (sample No. 4) are larger than sizes of particles obtained with fuel of other types.

The magnetization curves of the synthesized nanostructured powders were investigated using a vibrating sample magnetometer described in [4] for magnetizing fields in the range ±20 kOe at two temperatures: 80 and 295 K. Measurements were performed for spherical samples ≈1.8 mm in diameter. The spheres were produced from composites based on epoxy resin with 60 mass% of the synthesized powders. The hysteresis loops so obtained are shown in Fig. 1. From the figure it can be seen that sample No. 1 with the least content of the Ba-M phase and the greatest content of hematite, being a weak ferromagnet above the Morin temperature $T_M \approx 250$ K [5], has a lower value of the specific magnetization than other samples. Sample No. 4 has the highest value of magnetization. The magnetization curves in fields up to 20 kOe did not saturate. This demonstrates that in the processes of magnetization of the prepared nanostructured samples, the so-called process of true magnetization or the paraprocess can be important. The reasons for its occurrence in nanostructured hexaferrite powders are the following: a) the presence of nanoparticles of small sizes in superparamagnetic state in the synthesized samples; b) ordering of the spin magnetic moments with frustrated exchange bonds in the defective surface layer of nanoparticles in the magnetic field.

The main characteristics of the hysteresis loops are presented in Table 2. Values of the residual specific magnetization σ_r, determined at the point of intersection of the dependences $\sigma(H)$ with the ordinate when $H \to \pm 0$, are given in the second column.

The specific saturation magnetization $\sigma_{20\,kOe}$ was estimated in the maximal magnetic field $H = 20$ kOe. The ratios $2\sigma_r/\sigma_{20\,kOe}$ presented in Table 2 are close to 0.5. According to [6], this value is typical for magnetization processes of chaotically oriented single-domain particles of uniaxial magnets with magnetic ordering of the easy magnetization axis (EMA) type to which Ba-M hexaferrites belong. From Table 2 it follows that the coercive force increases with temperature. This demonstrates an increase in the value of the anisotropy field $H_a = 2k_1/M_S$ of the examined materials at

TABLE 2. Main Characteristics of the Hysteresis Loops

Sample No.	σ_r, G·cm^3/g	$\sigma_{20\ kOe}$, G·cm^3/g	$\sigma_r/\sigma_{20\ kOe}$, rel. units	H_c, kOe	σ_S, G·cm^3/g	$\chi_{para}\cdot10^3$, cm^3/g
80 K						
1	27.7	54.6	0.51	4.43	–	–
2	43.9	85.9	0.51	4.87	–	–
3	41.3	80.2	0.52	4.57	–	–
4	44.7	87.6	0.51	4.96	–	–
295 K						
1	18.7	38	0.49	4.96	37.5	0.133
2	28.5	56.6	0.5	5.49	57.2	0.115
3	28.1	55.4	0.51	5.27	56.2	0.125
4	29.8	59	0.5	5.63	59.5	0.125

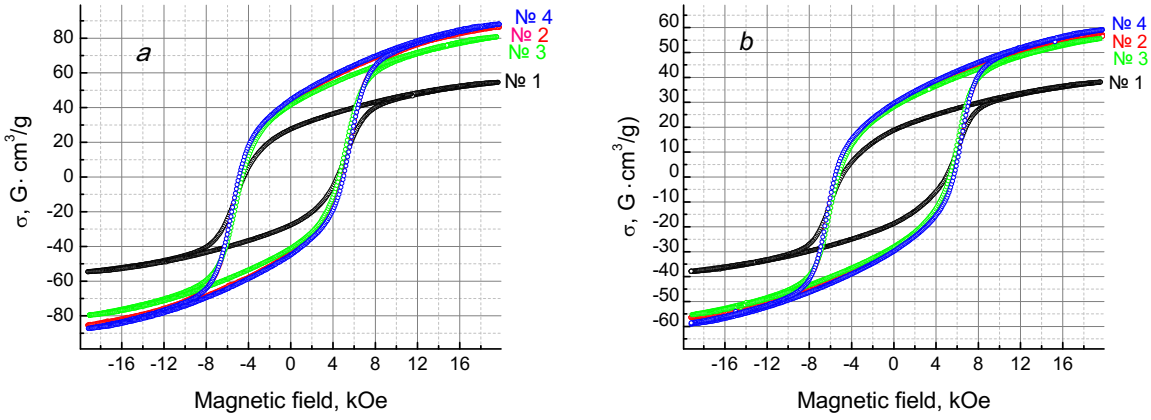

Fig. 1. Hysteresis loops of samples at temperatures of 80 K (*a*) and 295 K (*b*).

temperatures from 80 to 295 K. Here k_1 is the effective anisotropy constant, and M_S is the saturation magnetization of unit volume. Indeed, in [2] it was shown that at temperatures in the range specified above, the saturation magnetization of the massive Ba-M hexaferrite sample decreases with increasing temperature faster than the anisotropy constant k_1, that is, the anisotropy field H_{a1} increases.

Results of comparison of the experimental magnetization curves with calculated ones at a temperature of 295 K are shown in Fig. 2. The left panel shows sample No. 1, and the right panel is for sample No. 4. Symbols illustrate the experimental data for demagnetization sections of hysteresis loops from ±20 to ±0 kOe. The sections of the hysteresis loop in negative magnetizing fields were inverted for convenience of comparison from the third quadrant (see Fig. 1) to the first quadrant. The dashed curves show the dependence $\sigma_{calc}(H)$ calculated using the procedure described in Appendix 1. The values of the anisotropy fields H_{a1} used to calculate the magnetization curves were retrieved from the measured parameters of ferromagnetic resonance lines (Table 3).

The calculated curves in Fig. 2 were drawn as follows. The theoretical magnetization curves normalized by unity were multiplied by σ_S obtained by fitting of the theoretical curve at $H = 0$ to the experimental value of the specific residual magnetization σ_r. The σ_S values are given in the sixth column of Table 2. From the table it follows that they are close in values to $\sigma_{20\ kOe}$. As can be seen from Fig. 2, a noticeable discrepancy between the calculated and experimental curves is observed with increasing value of the magnetizing field. As noted above, the influence of the paraprocess can be a reason of this discrepancy. The contribution from the paraprocess susceptibility (χ_{para}) to the dependence $\sigma(H)$ was estimated from the formula

TABLE 3. Parameters of the Materials Measured by the Ferromagnetic Resonance Method

Sample No.	M_S, G	$\gamma/2\pi$, GHz/kOe	H_{a1}, kOe	α
1	198.0	2.80 ± 0.02	15.6 ± 0.1	0.07 ± 0.01
2	302.0	2.80 ± 0.02	15.0 ± 0.1	0.07 ± 0.01
3	296.7	2.80 ± 0.02	15.8 ± 0.1	0.10 ± 0.01
4	314.2	2.80 ± 0.02	15.4 ± 0.1	0.07 ± 0.01

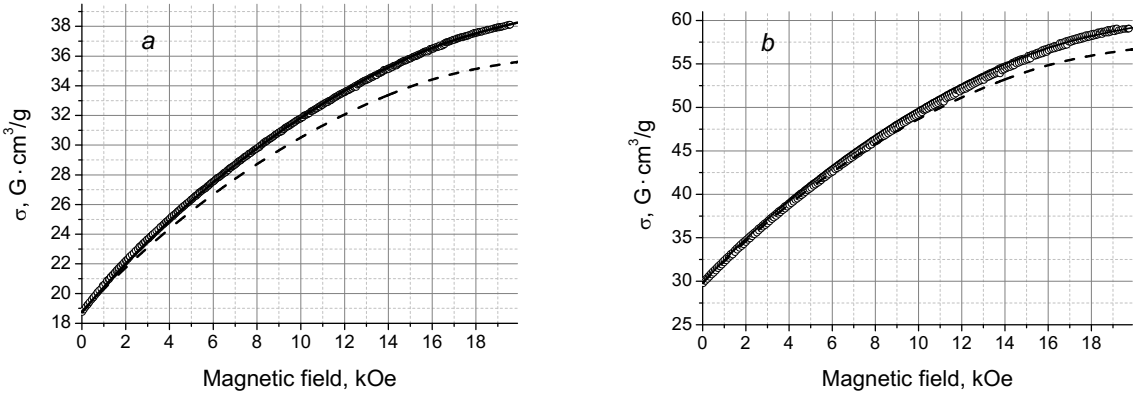

Fig. 2. Dependences $\sigma(H)$ for the demagnetization sections. Here symbols show experimental data and curves show the results of calculations for samples Nos. 1 (*a*) and 4 (*b*). The dashed curve (results of numerical calculations) describes the field dependence of the contribution from the processes of rotation of the magnetization vector $\sigma_{calc}(H)$ in $\sigma(H)$, and the solid curve describes the dependence $\sigma(H)$ taking into account the paraprocess.

$$\sigma(H) = \sigma_{calc}(H) + \chi_{para}H. \quad (1)$$

The obtained values of the susceptibility χ_{para} are given in the last column of Table 2, and the calculated dependences (solid curves) practically coincide with the experimental data.

Investigations of the ferromagnetic resonance (FMR) spectra of powder and polycrystalline oxide ferrimagnets with hexagonal crystal structure make it possible to determine experimentally a number of magnetic parameters of these materials important for practical applications, including values and signs of magnetocrystalline anisotropy fields along the hexagonal axis (H_{a1}) and in the basal plane (H_Θ) and the value of the effective magnetomechanic ratio $\gamma = ge/2mc$, where g is the effective g-factor of the examined material, e is the electron charge, m is the electron mass, and c is the velocity of light. The procedure of determining these parameters from FMR experiments is described in Appendix 2.

The FMR spectra were measured by the standard waveguide passing-through technique at frequencies in the range 37–53 GHz. To investigate the FMR, powders of the examined samples were put in thin-walled quartz tubes with inner diameter of 0.7 mm and length of 10 mm. The densities of powder samples were approximately the same and equal to ≈ 2.5 g/cm^3. The tubes were put in a rectangular waveguide parallel to its wide wall in order that the alternating magnetic field was directed along the sample axis. The constant magnetizing field was directed perpendicularly to the wide wall of the waveguide.

The experimental FMR data are shown by symbols in Fig. 3, and the imaginary parts of the diagonal components of the magnetic permeability tensor for samples Nos. 1–4 calculated in the approximation of independent grains are shown by the solid curves. The measurement frequency was 53 GHz. The experimental curves were normalized by theoretical ones.

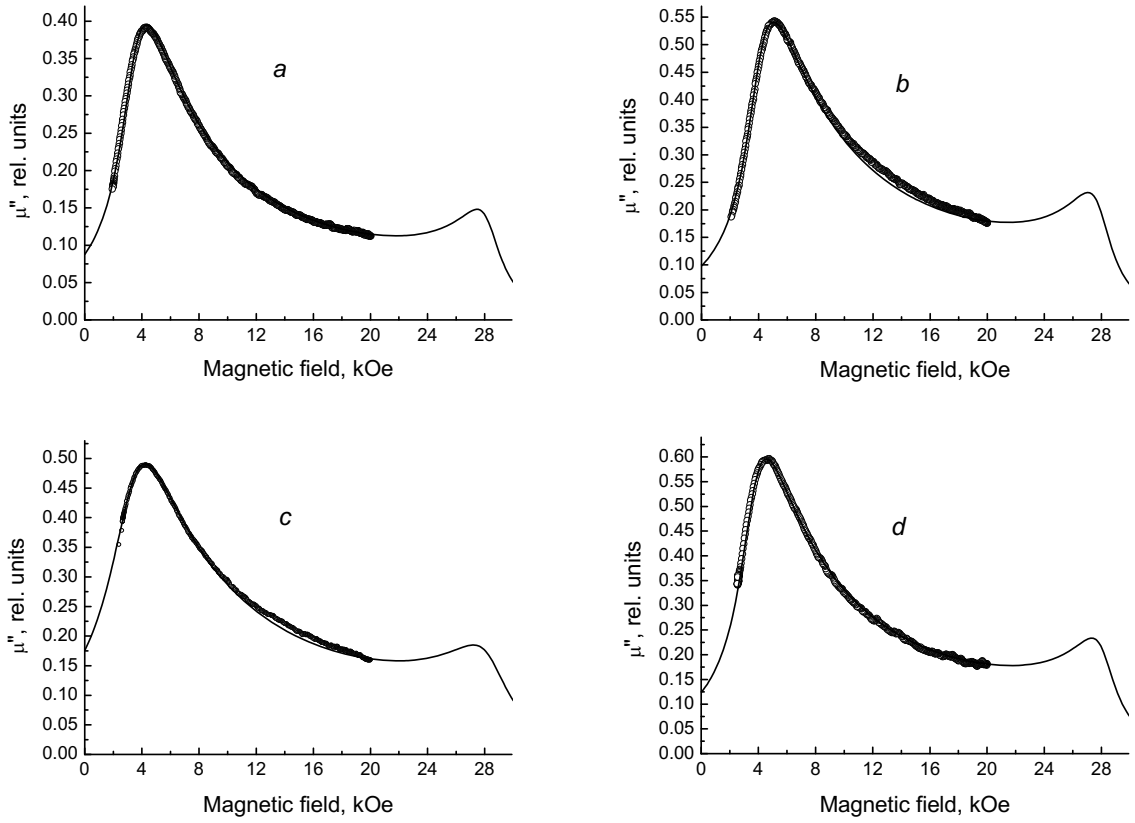

Fig. 3. Experimental (symbols) and calculated (solid curves) FMR curves for samples Nos. 1 (*a*), 2 (*b*), 3 (*c)*, and 4 (*d*) at a frequency of 53 GHz.

In the range of magnetizing fields accessible to us, only one maximum in the field close to $H_{\|}$ (see formula in Appendix 4) corresponding to the easy magnetization direction was observed experimentally. Therefore, from the experiment we estimated only values of the anisotropy field H_{a1} and effective magnetomechanic ratio γ. Values of the saturation magnetization of unit volume M_S necessary for calculation of the magnetic permeability tensor components were obtained from the formula $M_S = \sigma_S \rho$. Here ρ = 5.28 g/cm^3 is the x-ray density of Ba-M hexaferrite [2]. Values of the magnetomechanic ratios, anisotropy fields, and attenuation constants in the Landau–Lifshits–Hilbert equation are presented in Table 3.

According to Table 3, the measured values of the magnetomechanical ratios of the samples coincided within the experimental error with the magnetomechanical ratio for the free electron spin. The value of the effective anisotropy field of the samples depended on the organic fuel type. It was noticeably less than the data presented in the literature ($H_{a1} \approx 17$ kOe) for massive Ba-M hexaferrite samples [1, 2]. A possible reason is the influence of contributions from the particle shape anisotropy to H_{a1} [3] and from the magnetic anisotropy of the defective surface layer of nanoparticles [7].

Thus, our investigations of the influence of organic fuel type on the structural characteristics and magnetic properties of Ba-M hexaferrite powders synthesized by the zol-gel combustion method have demonstrated the following.

– Samples prepared using carbamide had the worst magnetic and structural characteristics both in the phase composition and value of the saturation magnetization.

– Smples prepared using citric acid had the largest particle sizes according to the CSR data, and the maximal value of the saturation magnetization.

– The paraprocess gave the noticeable contribution to the magnetization curves.

– The value of the effective magnetic anisotropy field depended on the organic fuel type.

APPENDIX 1. CALCULATION OF THE MAGNETIZATION CURVE OF CHAOTICALLY ORIENTED ELLIPSOIDAL PARTICLES WITH UNIAXIAL ANISOTROPY

Let us consider that the sample consists of chaotically oriented identical particles with uniaxial anisotropy of the EMA type. We consider that particles represent rotation ellipsoids whose rotation axis coincides with the hexagonal axis *c*. The density of the magnetic component of free energy (U) consists of contributions from the Zeeman energy (U_{Zee}), energy of particle demagnetizing field (U_{M}), and magnetocrystalline anisotropy energy (U_{MCA}). In spherical system of coordinates with the *z* axis coinciding with the hexagonal axis *c*, the free energy density is written as follows:

$$\begin{aligned} U &= U_{\text{Zee}} + U_{\text{M}} + U_{\text{MCA}} \\ &= -M_S H(\sin\Theta\sin\vartheta\cos(\Phi-\varphi)+\cos\Theta\cos\vartheta)+\left[2\pi M_S^2(N_\perp - N_\parallel)+k_1^{\text{MCA}}\right]\sin^2\vartheta. \end{aligned} \tag{A.1}$$

Here M_S is the saturation magnetization of unit volume; H is the external magnetizing field; $N_\perp$ and $N_\parallel$ are the transverse and longitudinal demagnetizing factors of the ellipsoid, and $2N_\perp + N_\parallel = 1$; k_1^{MCA} is the uniaxial magnetocrystalline anisotropy (MCA) constant; Θ and Φ are the polar and azimuthal angles of the magnetizing field; and ϑ and φ are the angles of the magnetization vector. To calculate the magnetization curve, the equilibrium orientation of the magnetization vector must be determined: equilibrium angles ϑ_0 and φ_0 must be found for preset value (H) and direction (Θ, Φ) of the magnetizing field. This problem was solved by minimizing the total energy U. Since the problem is cylindrically symmetric, $\varphi_0 = \Phi$, that is, the vectors ***M*** and ***H*** are coplanar. The equilibrium angle ϑ_0 is determined by the transcendental equation

$$H\sin(\vartheta_0 - \Theta) + 0.5H_{\text{a1}}\sin(2\vartheta_0) = 0\,. \tag{A.2}$$

Here $H_{\text{a1}} = 2k_1 / M_S = 2[k_1^{\text{MCA}} + 2\pi M_S^2(N_\perp - N_\parallel)] / M_S$, where k_1 is the effective anisotropy constant including contributions from the MCA and particle shape anisotropy. After numerical calculation of the dependence $\vartheta_0 = f(H, \Theta, H_{\text{a1}})$, the projection of the magnetization vector of a separate grain onto the magnetic field direction $M_H(H,\Theta) = M_S\cos(\Theta - \vartheta_0)$ can be calculated and then summed over all grains. It is natural that summation can be replaced by integration. This problem can be solved most simply for the demagnetization curves shown in Fig. 2. In this case, the magnetization vectors of all grains and the magnetizing field are in the upper half-plane, and the angles Θ and ϑ_0 change from 0 to π/2. The magnetization curve of the powder sample was calculated from the formula

$$M_H(H) = \int_0^{\pi/2} M_H(H,\Theta)\sin(\Theta)d\Theta\,. \tag{A.3}$$

Results of calculations of the magnetization curves in relative units ($M_H(H)/M_S$) using this procedure for the indicated values of the field anisotropy are shown in Fig. A1.

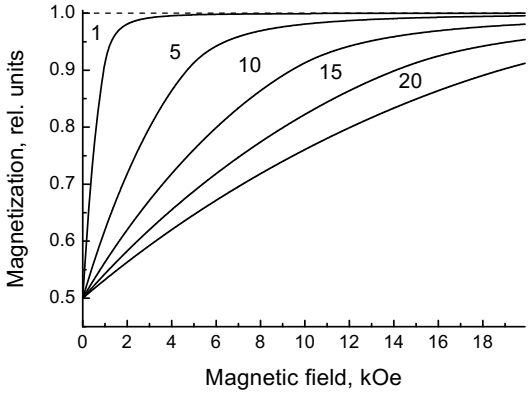

Fig. A1. Magnetization curves calculated for the indicated values of the anisotropy fields. Figures adjacent to the curves indicate the values of the anisotropy fields, H_{a1}, in kOe.

APPENDIX 2. DETERMINATION OF VALUES OF THE ANISOTROPY FIELDS OF UNIAXIAL MATERIALS WITH EMA FOR POLYCRYSTALLINE AND POWDER SAMPLES FROM THE FMR EXPERIMENT

For powder and polycrystalline hexaferrites with high MCA field, the approximation of independent (or noninteracting) grains is well fulfilled. The principles of FMR theory for such materials were formulated by E. Schlömann [8, 9]. In [10] this theory was generalized to the media with anisotropic magnetomechanical ratio γ. A disadvantage of the calculation methods presented in [8–10] is the impossibility of calculation of the FMR curve for uniaxial materials with EMA at frequencies lower than the frequency of natural ferromagnetic resonance (NFMR): $\omega_{NFMR} = \gamma H_{a1}$. This disadvantage has been overcome in [11] where the method for calculation of the components of the magnetic permeability tensor for uniaxial single-domain polycrystalline and powder materials for arbitrary frequencies was suggested. In [8–11] it was demonstrated that the FMR curves (illustrating the field dependences of the imaginary parts of the magnetic permeability components) have two special features: maxima and (or) steps. The special features of the FMR curves are observed in the vicinities of $H_{\parallel}$ and $H_{\perp}$ magnetizing field values corresponding to the stationary directions in the angular dependence of the resonant field of a single crystal grain. The values of the resonant fields (or frequencies) are given by the formulas [10–12]

$$\omega_{\parallel} = \gamma\left[H_{\parallel} + H_{a1}\right], \quad \omega_{\perp} = \gamma\left[H_{\perp}\left(H_{\perp} - H_{\Theta}\right)\right]^{1/2}, \quad \omega_3 = \gamma\left[H_{a1}^2 - H^2\right]^{1/2}. \tag{A.4}$$

Here $\omega_{\parallel}$ and $\omega_{\perp}$ are resonant frequencies for the directions along the hexagonal axis *c* of the crystal lattice ($\Theta = 0$) and in the basal plane ($\Theta = \pi/2$), respectively. The resonance at the frequency ω_3 is observed at frequencies lower than ω_{NFMR} when the resonance at the frequency $\omega_{\parallel}$ does not exist. Formulas (A.4) are written under assumption that the higher-order MCA constants can be neglected in comparison with k_1^{MCA}. In this case, the value of the anisotropy field in the basal plane is $H_{\Theta} = H_{a1}$. The field dependences of the resonant frequencies calculated from formulas (A.4) for $\gamma = 2.8$ GHz/kOe and $H_{a1} = 10$ kOe are shown in Fig. A2. The dashed curves in Fig. A2 indicate the frequencies at which the resonant curves of the polycrystal shown in Fig. A3 were calculated. Figures adjacent to the curves indicate frequencies, in GHz. Vertical bars in Fig. A3 indicate values of the fields calculated from formulas (A.4) for the corresponding directions.

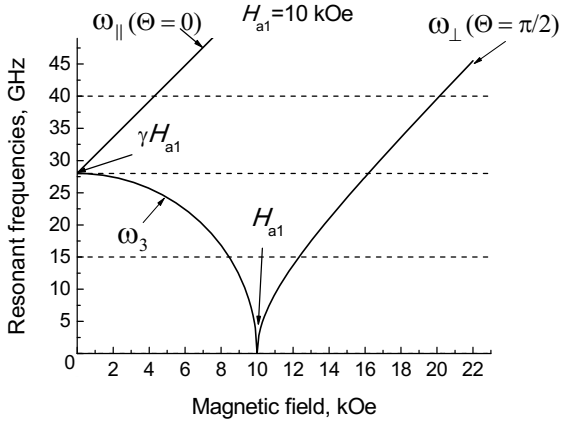

Fig. A2

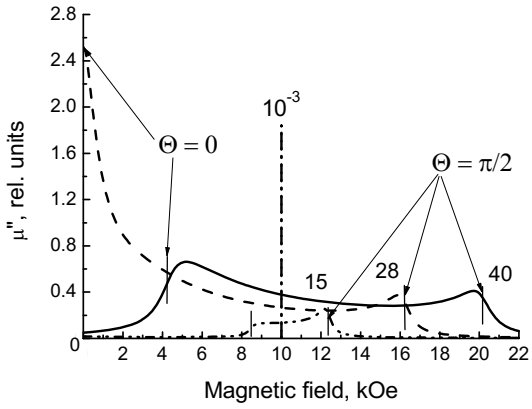

Fig. A3

Fig. A2. Field dependences of the branches of the resonant frequency spectrum for the material with EMA along the directions of easy ($\omega_{\|}$ $\Theta = 0$) and hard ($\omega_{\perp}$ $\Theta = \pi/2$) magnetization at the frequency ω_3.

Fig. A3. Resonant curves of a polycrystal calculated for the parameters H_{a1} = 10 kOe, M_S = 0.3 kG, and the attenuation constant $\alpha = 0.05$. Figures adjacent to the curves indicate frequencies, in GHz.

The resonant peak intensity at a frequency of 10^{-3} GHz was reduced by 100 times. In fact, it represents the jump of the imaginary part of the permeability at the point of magnetization reversal (the magnetization vector in this case lies in the hard magnetization plane).

From Fig. A3, we can conclude the following about the method of determining the anisotropy fields from the FMR experiments.

1. It is better to investigate the FMR spectra at the frequencies $\omega > \gamma H_{a1}$ since in this case, the imaginary part of the magnetic permeability is higher than for $\omega < \gamma H_{a1}$.

2. The experimental FMR spectra must be processed in two stages. In the first stage, the frequency dependences of the resonant fields are constructed for the directions of easy and hard magnetizations. Then values of the magnetomechanic ratio γ and anisotropy fields H_{a1} and H_{Θ} are calculated from formulas (A.4) for $\omega_{\|}$ and $\omega_{\perp}$ by the least squares method. In the second stage, the refined values of these parameters are estimated by detailed comparison of the experimental and calculated resonant curves at different frequencies.

The work on synthesis of the materials was supported in part by the Federal Agency for Scientific Organizations of Russia (Project V.44.3.4 No. AAAA-A17-117070420014-9). The measurement of magnetic and structural parameters of the materials was supported in part by the Program for Increasing TSU Competitiveness among the Leading World Scientific-Educational Centers and the Russian Foundation for Basic Research (Grant No. 16-03-00256).

REFERENCES

1. R. C. Pullar, Prog. Mater. Sci., **57**, 1191–1334 (2012).
2. J. Smit and H. P. J. Wijn, Ferrites [Russian translation], Inostrannaya Literatura, Moscow (1958).
3. E. P. Naiden, V. A. Zhuravlev, R. V. Minin, et al., Russ. Phys. J., **58**, No. 1, 125–132 (2015).
4. D. A. Velikanov, Vestn. SibGAU, No. 1 (53), 147–154 (2014).
5. F. J. Morin, Phys. Rev., **78**, No. 6, 819 – 820 (1950).
6. E. C. Stoner and E. P. Wohlfart, IEEE Trans. Magn., **27**, No. 4, 3475–3518 (1991).

7. S. P. Gubin, Yu. A. Koksharov, G. B. Khomutov, and G. Yu. Yurkov, Usp. Khim., **74**, 539–574 (2005).
8. E. Schlömann, J. Phys. Chem. Solids, **6**, 257–266 (1958).
9. E. Schlömann and R. V. Jones, J. Appl. Phys., **30**, S177–S178 (1959).
10. V. A. Zhuravlev, Fiz. Tverd. Tela, **41**, No. 6, 1050–1053 (1999).
11. V. A. Zhuravlev and V. A. Meshcheryakov, Russ. Phys. J., **56**, No. 12, 1387–1397 (2013).
12. E. P. Naiden, V. A. Zhuravlev, V. I. Itin, *et al*., Russ. Phys. J., **55**, No. 8, 869–877 (2012).